Persistent eastern equatorial Pacific Ocean upwelling since the warm Pliocene

Patrick A. Rafter[1,2]*†, Jesse R. Farmer[3,4,5]*†, Alfredo Martínez-García[5], A. C. Ravelo[6], Kristopher B. Karnauskas[7,8], Fabian C. Batista[6], Stefano M. Bernasconi[9], Haojia Ren[10], Alexandra Auderset[11], Gerald H. Haug[5,9], & Daniel M. Sigman[4]

[1] College of Marine Science, University of South Florida, 830 1st Street S, St. Petersburg FL 33701 USA

[2] Department of Earth System Science, UC Irvine, Irvine, USA

[3] School for the Environment, University of Massachusetts Boston, 100 Morrissey Blvd., ISC 2110, Boston MA 02125 USA

[4] Department of Geosciences, Princeton University, Guyot Hall, Princeton, NJ 08544 USA

[5] Department of Climate Geochemistry, Max Planck Institute for Chemistry, Hahn-Meitner-Weg 1, 55128 Mainz, Germany

[6] Ocean Sciences Department, UC Santa Cruz, Santa Cruze, USA

[7] Department of Atmospheric & Oceanic Sciences, University of Colorado Boulder, Boulder, USA

[8] Cooperative Institute for Research in Environmental Sciences, University of Colorado Boulder, USA

[9] Department of Earth and Planetary Sciences, ETH Zürich, Zürich, Switzerland

[10] National Taiwan University, Taipei, Taiwan

[11] University of Southampton, Southampton, UK

*Corresponding authors. Emails: prafter@usf.edu, jesse.farmer@umb.edu

† These authors contributed equally to this work

Abstract: Upwelling generates a nutrient-rich "cold tongue" in the eastern equatorial Pacific Ocean (EEP), with impacts on global climate, oceanic biological productivity, and the carbon cycle. The cold tongue was reduced during the Pliocene Epoch, a feature attributed to weaker upwelling and an associated deepening of the surface mixed layer in the EEP. Here, we report nitrogen-isotope evidence that modern-like upwelling occurred in the EEP during the Pliocene and has persisted over the last 5 million years. We explain the reduced Pliocene cold tongue as an expression of the reduced temperature difference between surface and subsurface waters in the tropical Pacific. The attendant reduction in the vertical density gradient may have maintained EEP upwelling despite the expected slackening of the trade winds under Pliocene warmth.

Main Text: In the tropical Pacific Ocean, warm ocean waters in the surface mixed layer (ML) are separated from the ocean interior by the thermocline, the strongest temperature (and thus density) gradient of the water column (Fig. 1A). Starting just below the base of the ML, the concentrations of nutrients increase downward through the thermocline; this vertical nutrient

gradient is known as the nutricline. Below the thermocline (below roughly 500 m, defined here as the "subthermocline") are mode and intermediate waters, which extend down to a depth of ~1200 m and are characterized by a much more gradual downward decrease in temperature, and are underlain by the deep ocean.

The tropical easterly trade winds shoal the eastern equatorial Pacific (EEP) thermocline, allowing cool, nutrient-bearing thermocline water to upwell to the surface and create both a "cold tongue" and a "nutrient tongue" in the EEP (Fig. 1, B and C). Alterations to EEP upwelling and thermocline depth impact local marine ecosystems (*1*), and atmospheric teleconnections driven by changes in the zonal sea surface temperature (SST) gradient affect climate (*2*). For example, the interannual weakening of trade winds during the El Niño phase of El Niño-Southern Oscillation (ENSO) causes the EEP cold tongue and nutrient tongue to temporarily disappear (*1*), with reductions in EEP fisheries (*1,3*) and globally distributed climatic effects (*4*).

The Pliocene Epoch [5.33 to 2.6 million years ago (Ma)] is considered a paleoclimate analog for Earth's climate in the upcoming decades to centuries (*5,6*). Seawater temperature reconstructions from the equatorial Pacific back into the Pliocene (Fig. 2A; see Materials and methods) provide insight into how this climatically important region behaves in a warmer world. Reconstructions of SST in the western equatorial Pacific (WEP) and EEP (Fig. 2A) indicate that, during the Pliocene, the EEP cold tongue was warmer (*7-9*) and, despite some debate (*10,11*), that the zonal SST gradient was reduced (*9, 12-15*). Given equatorial Pacific SST-wind-upwelling feedbacks (*16,17*), the smaller Pliocene zonal SST gradient is expected to have been accompanied by weaker upwelling and a deeper ML (i.e., a deepening of the top of the thermocline) in the EEP. It has also been proposed that warming of extratropical waters deepened the base of the EEP ML during the Pliocene (*18*). Reconstructions from the EEP suggest that the temperatures of both the surface and the shallow subsurface (~100 m depth) were elevated during the Pliocene (*19,20*). In detail, the reconstructed warming was greater in the shallow subsurface than in the ML (*20*) (Fig. 2A). The implied reduction in the surface-to-shallow subsurface temperature gradient would appear to support the interpretation of a deeper EEP ML during the Pliocene, although other interpretations are possible.

A robust relationship is observed between temperature and nutrients in the modern tropical Pacific in both space and time (*1*). Thus, the reduced cold tongue during the Pliocene would appear to predict a reduced nutrient tongue as well. However, reconstructions indicate that biological export production in the Pliocene EEP was similar to or even higher than today (Fig. 2, B and C), suggesting that nutrient supply to the EEP ML was not lower during the Pliocene (*7,8,21-24*). Here, we use nitrogen (N) isotopes to test for Plio-Pleistocene changes in the upwelling of nutrient-rich waters to the EEP euphotic zone, the photosynthetically active upper layer that includes the ML. We measured the ^{15}N-to-^{14}N ratio (expressed as $\delta^{15}N$) of bulk sedimentary and planktonic foraminifera-bound organic matter ($\delta^{15}N_{sed}$ and FB-$\delta^{15}N$, respectively) in equatorial Pacific sediments extending back to the warm Pliocene ($\delta^{15}N = ((^{15}N/^{14}N)_{sample}/(^{15}N/^{14}N)_{reference} - 1)*1000‰$, where the reference is air N_2). Specifically, $\delta^{15}N_{sed}$ records the $\delta^{15}N$ of N that sinks from the surface ocean, which in turn approximates the $\delta^{15}N$ of nitrate consumed in surface waters (*25*). Core-top studies indicate that FB-$\delta^{15}N$ also reflects the

δ^{15}N of nitrate consumed (*26,27*). Both proxies, however, have additional controls that might cause deviations from a constant relationship. The δ^{15}N of organic matter in sediments can be increased by microbial degradation (*25,28*), and organic N carrying a different δ^{15}N value can also enter the sediments from outside the marine system of interest (*28*); these effects can change over time and as a function of environmental conditions. FB-δ^{15}N is species-specific, with euphotic zone-dwelling species that bear photosynthetic endosymbionts having a δ^{15}N close to the nitrate consumed in their ecosystem (*26,29*). In modern upper ocean studies, seasonal variations in FB-δ^{15}N independent of nitrate consumption have been observed (*29,30*), raising the possibility of such behavior affecting the δ^{15}N of the annually integrated flux of a given foraminifera species to the seafloor. Since $\delta^{15}N_{sed}$ and FB-δ^{15}N have different sources of uncertainty, consistency between these proxies greatly increases confidence in observed changes and their interpretation.

A comparison of δ^{15}N records from core sites with different longitudes across the equatorial Pacific allows for separation of the effects of (i) the δ^{15}N of the equatorial thermocline nitrate supply from (ii) the degree of nitrate consumption in the surface waters above each core site (*31*). In most low and midlatitude ocean regions, nitrate delivered from the subsurface by upwelling or mixing is completely consumed by phytoplankton, and the δ^{15}N of the nitrate consumed in (and therefore the organic N exported from) surface waters is equal to the δ^{15}N of the subsurface nitrate source. Ocean Drilling Program (ODP) Site 806 in the WEP (0.3° N, 159.4° E) is in such a region (Fig. 1A,C). Thus, we measure $\delta^{15}N_{sed}$ and FB-δ^{15}N at Site 806 to reconstruct the δ^{15}N of the equatorial thermocline nitrate supply over the past 5 Myr. In contrast, in surface waters with incomplete nitrate consumption, such as the EEP nutrient tongue (Fig. 1), the preferential consumption of ^{14}N-nitrate leads to sinking organic matter δ^{15}N that is lower than the δ^{15}N of nitrate supply (*25*) (fig. S1). EEP-located ODP Site 849 (0.2° N, 110.5° W) captures such conditions (Fig. 1A,C). Because the δ^{15}N of thermocline nitrate upwelled in the WEP and EEP is similar (*32,33*), and because WEP Site 806 within the nitrate-free Western Pacific Warm Pool is unlikely to have ever been characterized by significant surface nitrate concentrations, changes in the δ^{15}N difference between the WEP and EEP indicate changes in surface nitrate consumption in the EEP (*31*). This interpretation is quantitatively supported by our data. Based on equatorial Pacific nitrate concentration and δ^{15}N measurements (*32,33*) (fig. S1), the modern δ^{15}N of nitrate consumed in the WEP is 4.1±0.5‰ (1 standard deviation) higher than in the EEP (Materials and Methods). This difference is reflected in $\delta^{15}N_{sed}$ and FB-δ^{15}N over the Holocene, with WEP $\delta^{15}N_{sed}$ and FB-δ^{15}N values elevated relative to the EEP by 4.4±0.8‰ and 3.8±1.1‰, respectively (Fig. 3A).

In both $\delta^{15}N_{sed}$ and FB-δ^{15}N and at both sites, the records are characterized by a ~5‰ increase over the past 5 Myr (Fig. 3A), with the δ^{15}N difference between WEP and EEP exhibiting long-term stability at >100 thousand years (kyr) (i.e., greater-than-orbital) time scales (Fig. 3C). The similarity of the changes in $\delta^{15}N_{sed}$ and FB-δ^{15}N proxy records at both sites supports the reliability of both N isotope proxies over the last 5 Myr (Materials and methods). In the next

sections, we first address the significance of the long-term stability in the WEP-to-EEP $\delta^{15}N$ difference for tropical Pacific dynamics since 5 Ma. We then consider the possible origins of the $\delta^{15}N$ increase over this time that is shared between the WEP and EEP records (Fig. 3A).

Equatorial Pacific zonal $\delta^{15}N$ gradient and EEP upwelling

By using 200 kyr LOESS filters to estimate long-term trends (Materials and Methods), the WEP-EEP $\delta^{15}N$ difference in bulk sedimentary N ($\Delta\delta^{15}N_{sed}$) averages 3.8±0.7‰ over the past 5 Myr (Fig. 3). Similarly, the WEP-EEP difference in foraminifera-bound $\delta^{15}N$ (ΔFB-$\delta^{15}N$) averages 3.9±0.6‰ over the past 5 Myr (fig. S1). On the timescales of >100 kyr investigated here, the zonal gradients in both proxy records are indistinguishable from the expected modern WEP-EEP sinking organic matter $\delta^{15}N$ difference of 4.1±0.5‰ (Materials and methods). Thus, the N isotope data indicate that the modern zonal gradient in equatorial Pacific surface nitrate concentrations, driven by EEP upwelling, has been a persistent feature of the past 5 Myr.

Tropical Pacific temperature reconstructions indicate a reduced Pliocene zonal SST gradient (*9, 12-15*) (Fig. 2A), which has been interpreted to indicate a weakening of the cold tongue and a deepening of the ML in the EEP associated with weaker upwelling of thermocline water (*9,19*). These changes would have reduced the nitrate supply to the EEP euphotic zone, resulting in more complete consumption of nitrate by phytoplankton and a reduced EEP nutrient tongue during the Pliocene. The N isotopes should have recorded such a change as a reduced WEP-to-EEP $\delta^{15}N$ gradient ($\Delta\delta^{15}N$ values lower than the observed late Pleistocene value of ~4‰, Fig. 3C). Instead, the N isotope data indicate an EEP nutrient tongue over the past 5 Myr, conflicting with the above expectations and calling for persistent upwelling in the EEP over the Plio-Pleistocene (*24*).

In the low-latitude water column, the shallowest occurrences of the thermocline and nutricline are tightly coupled, both occurring at the base of the ML (Fig. 1A). This coupling reflects that, if nutrients are injected into the waters above the thermocline, they are now within the warm, buoyant ML and cannot be prevented from mixing to the surface, where they will be consumed by phytoplankton. For the same reason, any remineralization of sinking organic matter above the thermocline (i.e., within the ML) is immediately accessible to phytoplankton in the surface (i.e., it becomes part of "recycled production"), such that it will be re-assimilated and re-exported until it sinks below the base of the ML, driving an inherent coupling between the thermocline and nutricline (*34*). Thus, the presence of an EEP nutrient tongue requires upwelling of water from the thermocline during the Pliocene, exposing sub-ML water at the EEP surface.

Despite previous interpretations of weaker EEP upwelling to explain Pliocene SST proxy data, subsurface temperature proxy data would appear to support the N-isotope data in arguing against such weaker EEP upwelling. During the Pliocene, while both SSTs and shallow subsurface temperatures were warmer relative to present day (Fig. 2A), the data indicate that there has been a surface-to-shallow subsurface temperature gradient in the EEP since 5 Ma (*9,19,24*) (Fig. 2).

Accordingly, the base of the ML must have remained above an ~100 m depth in the EEP. This would allow upwelling to import thermocline water with high nutrient concentrations to the ML, as the N-isotope data require.

Thermocline, mode, and intermediate waters in the tropical Pacific subsurface are derived from the high-latitude surface ocean, which experienced amplified warming relative to the tropical Pacific surface during the Pliocene (*13,14*) (fig. S5). This amplification was part of a global-scale decrease in the equator-to-pole temperature gradient and, thus, in the tropical surface-to-deep temperature gradient (*19,20,35,36*). With this decrease in temperature gradients, the thermocline would have been defined by less distinct temperature extremes (*20*). In contrast, the default expectation for the ocean nutrient reservoir is that it has been stable from the Pliocene to the present (*37*). With a weaker thermocline but a similar-to-modern nutricline during the Pliocene, the EEP cold tongue would have been reduced during the Pliocene, whereas the nutrient tongue would have been similar to that of modern times, as the data indicate (solid arrow in Fig. 4A). In contrast, a decrease in upwelling would have both raised the temperature and decreased the surface nitrate concentration in the EEP, counter to the observations (dashed arrow in Fig. 4A). Thus, the combined Pliocene temperature and N-isotope data are consistent with similar-to-modern EEP upwelling in the context of a weaker-than-modern tropical Pacific thermocline.

Commented [JF1]: Good update here - it's more clear and gets us away from saying "no change," which was dangerous

Numerical models simulate a weakening of the tropical easterly trade winds under global warming and in warmer climates in general (*12*), which would have weakened wind-driven upwelling in the EEP and worked to reduce the zonal tilt in the tropical thermocline during the warm Pliocene. However, warmer Pliocene interior waters would have weakened the thermocline and thus the pycnocline (the vertical density gradient) (*13*), reducing the potential energy barrier to the upwelling and turbulent mixing of nutrient-bearing thermocline water into the mixed layer-(*38*). This reduced stratification would have facilitated more efficient entrainment of thermocline water into the mixed layer, countering the effect of reduced wind forcing in terms of the Richardson number. A simple box model of Ekman pumping damped by stratification for a range of such parameters spanning the Pliocene to modern (Fig. 4B) demonstrates that the weaker pycnocline in the Pliocene would have at least partially compensated for weaker trade winds, so as to maintain the total upwelling and entrainment of subsurface water and nutrients into the ML. Additionally, theoretical and numerical studies indicate that reduced stratification can deepen the source depth of upwelled waters, potentially enhancing the nutrient supply to the euphotic zone (*39*). Thus, on > 100 kyr timescales, the Pliocene Pacific's weaker thermocline may have maintained the rate of EEP upwelling despite weaker trade winds (Fig. 4).

Commented [JF2]: I think we should specify that we are talking about > 100 kyr timescales in this sentence. This statement may not be true on precessional timescales, for instance

Equatorial Pacific nitrate $\delta^{15}N$ and Plio-Pleistocene denitrification change

On timescales of >5000 years, the $\delta^{15}N$ of thermocline nitrate in the Pacific should be controlled largely by the isotopic characteristics of the global ocean's fixed N budget and not by changes in the high-latitude sources of nitrate to thermocline waters (*40*). Fixed N is added to the ocean predominantly through the microbial fixation of dinitrogen gas and is removed largely by

microbial denitrification in environments where dissolved oxygen is nearly completely consumed (i.e. < 5 µmol kg^{-1}): in certain marine sediments and in the oxygen-deficient zones (ODZs) that occur in the ocean's tropical thermocline, mostly in the eastern tropical Pacific. The isotopic fractionations associated with these inputs and outputs alter the $\delta^{15}N$ of nitrate within the thermocline. Newly fixed N has a $\delta^{15}N$ of ~-1‰, and its remineralization lowers the $\delta^{15}N$ of nitrate in the tropical and subtropical thermoclines (*41*). In contrast, water column denitrification preferentially removes ^{14}N-nitrate and thus raises the $\delta^{15}N$ of residual nitrate within the ODZs (*42*). This isotopic signal is circulated through the tropical Pacific thermocline (*32,33*) and eventually through the global ocean (*43*). Unlike water column denitrification, sedimentary denitrification does not strongly increase the $\delta^{15}N$ of oceanic fixed nitrogen (*43*). As a result, the global average $\delta^{15}N$ of nitrate in the combined thermocline, mode, and intermediate water is principally set by the proportion of denitrification occurring within the water column versus the sediments (*40,43,44*).

Given these isotope systematics, the Plio-Pleistocene $\delta^{15}N$ rise shared between WEP and EEP ODP Sites 806 and 849 (Fig. 3) has two possible origins. First, it may reflect a decline in sedimentary denitrification, which would have caused water column denitrification to account for an increasing fraction of total denitrification over the Plio-Pleistocene. Second, it may reflect a rise in water column denitrification. Either alternative would have caused an increase in the $\delta^{15}N$ of thermocline water nitrate. Because the Pacific accounts for most of the global ocean's water column denitrification, a Plio-Pleistocene rise in water column denitrification would have caused the strongest $\delta^{15}N$ increase in Pacific thermocline water (*44*), which influences the nitrate supplied to the euphotic zone and ML above Sites 806 and 849 (Fig. 1).

To distinguish between these alternatives, we considered FB-$\delta^{15}N$ data from DSDP Site 516 in the subtropical South Atlantic (30.3°S, 35.3°W), which tracks the $\delta^{15}N$ of nitrate in the region's thermocline (*45,46*). In contrast to the long-term $\delta^{15}N_{sed}$ and FB-$\delta^{15}N$ increases at tropical Pacific Sites 806 and 849, South Atlantic Site 516 FB-$\delta^{15}N$ shows no long-term change over the last 5 Myr (Fig. 3B). This contrasting behavior between Pacific and Atlantic $\delta^{15}N$ favors a mechanism that increased thermocline nitrate $\delta^{15}N$ only in the Pacific: An increase in tropical Pacific water column denitrification over the Plio-Pleistocene. In this case, any associated global Plio-Pleistocene thermocline nitrate $\delta^{15}N$ signal must have been either small or alternatively countered by other local processes in the South Atlantic so as to yield a stable FB-$\delta^{15}N$ at Site 516. One possibility is that the N_2 fixation rate increased in the South Atlantic in response to enhanced water column denitrification in the tropical Pacific (*47,48*), thereby lowering the thermocline nitrate $\delta^{15}N$ in the South Atlantic subtropical gyre relative to the global pycnocline average $\delta^{15}N$. An increase in the extent of the Pacific ODZs since the warm Pliocene is further supported by observed increases in $\delta^{15}N$ proxies proximal to the Pacific ODZs from the Late Miocene (*37*) through the early Pleistocene (*48,49*) (fig. S3). In summary, the lower $\delta^{15}N_{sed}$ and FB-$\delta^{15}N$ in the tropical Pacific during the warm Pliocene represents additional evidence that the ocean's ODZs tend to be smaller in globally warmer climates (*37,45,48-52*).

A weakened Pliocene Pacific ODZ occurred despite evidence for lower pH in the EEP mixed layer (*23*). Shankle et al. (*23*) interpreted the lower EEP pH to indicate the upwelling of older subsurface water with a higher concentration of regenerated nutrients. However, such a change would have been accompanied by a reduction in oxygen concentration (*53*). This runs contrary to our findings of reduced water column denitrification and thus better oxygenation of thermocline water in the Pliocene tropical Pacific. This apparent disagreement might be explained by the sensitivity of seawater pH to other conditions. In particular, calculations indicate that much of the pH reduction observed in the Pliocene EEP (*23*) can be explained by the dependence of pH on temperature (Materials and methods and fig. S4). If so, the reconstructed reduction in EEP pH of the Pliocene does not require an increase in either the regenerated nutrient concentration of EEP thermocline water or the EEP upwelling rate.

In climate model experiments, the spatial extent of Pacific ODZs is affected by a range of factors (*54-59*): (i) the initial oxygen concentration of high latitude source waters that ventilate the low latitude thermocline, largely controlled by temperature; (ii) the rate and source water proportions of that thermocline ventilation; (iii) the oxygen demand due to remineralization within thermocline water, jointly controlled by the initial nutrient concentration of their high latitude source waters (*55*) and the strength of tropical upwelling [e.g., through trade wind strength (*60*)]; and (iv) the oxygen content of underlying deep waters, which mix with and upwell into the tropical thermocline (*58,61*). Warmer Pliocene waters would reduce the solubility of dissolved oxygen, lowering the initial oxygen concentrations of high latitude source waters. Moreover, based on the continued nutrient upwelling in the EEP and the similar or higher-than-modern productivity during the Pliocene (Fig. 2, B and C, and 3), the oxygen demand for sinking organic matter remineralization should be maintained. Finally, the higher temperatures would have encouraged shallow remineralization of sinking organic matter (*62*). All of these changes would strengthen the ODZ, in contrast to the $\delta^{15}N$ observations. Additionally, continued productivity and nutrient upwelling in the Pliocene EEP is not compatible with a reduction in preformed nutrients in southern-sourced waters in a warmer climate, arguing against this potential cause of ODZ contraction.

By elimination, a change in the ventilation of the thermocline, intermediate, and/or deep ocean is implicated as the cause of the Pacific ODZ contraction during the Pliocene. There are contrasting views regarding North Pacific mode-, intermediate-, and deep-water formation during the Pliocene (*23,63,64*), but ventilation from one of these sources may have been stronger (*53,63,64*). In addition, the Antarctic may have driven stronger deep ocean ventilation (*65*). Numerical models vary in the connections that they predict between global climate and the intermediate- and mode-water ventilation of the tropical thermocline [e.g., (*66*)]. With regard to the deep ocean, the warmer Pliocene climate may have encouraged ventilation through a poleward shift in the westerly winds (*67*) or thermohaline effects (*65,68,69*). Thus, the lower surface-to-deep temperature difference during the warm Pliocene, which we have implicated in the persistence of the EEP upwelling, may also have played a role in the smaller Pacific ODZ of the warm Pliocene.

Implications

The persistence of eastern equatorial Pacific upwelling throughout the last 5 Myr has implications for the drivers of Pliocene warmth and Plio-Pleistocene cooling. On the basis of warmer upwelling regions, it has been argued that the Pliocene hosted a deeper EEP thermocline, with its subsequent shoaling over the Plio-Pleistocene facilitating the onset of the glacial-interglacial cycles that dominated the Pleistocene (*18*). The N-isotope data demonstrate that the amplified cooling of the EEP since the Pliocene was not associated with the emergence of its modern nutrient tongue. The existence of the EEP nutrient tongue during the Pliocene indicates that the ML depth and upwelling rate of the Pliocene EEP were similar to those of the modern state. Coming toward the present, stronger cooling of the subthermocline relative to the tropical Pacific surface is the only Plio-Pleistocene change required to simultaneously explain the temperature and N-isotope proxy data (Fig. 4). Thus, our study argues against an increase in EEP upwelling rate as a key driver of Plio-Pleistocene cooling.

The evidence presented here for a similar-to-modern ML depth in the Pliocene EEP, when combined with prior evidence of a deeper ML in the WEP (*20,70*), implies a steeper east-to-west tilt of tropical Pacific ML depth during the Pliocene, counter to proposals of the opposite (*9*). These observations raise the possibility that, in the case of a reduced vertical density gradient in the tropical ocean, any given seawater density surface may be subject to greater slopes, owing to the reduced gravitational potential energy associated with such slopes in an ocean with weaker density variation. This effect on the slopes of density surfaces may be important for ocean circulation and for spatial patterns in nutrient supply to surface waters under different climates, warranting further investigation.

With regard to the future, our findings raise the possibility that the coincident tendencies of global warming to weaken the trade winds and the density stratification of the tropical thermocline will counteract one another, resulting in relatively stable equatorial upwelling in the face of climate change, at least once thermocline, mode, and intermediate waters have equilibrated with the warmer climate (Fig. 4B). As a caveat to this interpretation, studies of the Middle Miocene Climate Optimum and Paleocene-Eocene Thermal Maximum, which were even warmer than the Pliocene, suggest that EEP upwelling may have been reduced at those times (*45,50,51*). The combined findings suggest that the equatorial Pacific nutrient tongue can disappear under very warm climates, but that the Pliocene had not reached that threshold. If so, a reduction in EEP upwelling may only occur if future global warming is so intense that the reduction in the vertical ocean density gradient is no longer adequate to offset the effect of weaker easterly trade winds.

Our results also have implications for future oxygenation of the subsurface tropical Pacific Ocean. In some global warming model simulations, ODZs contract because a reduced influx of older, deeper water—and thus greater incursion of better ventilated, lower-density, shallower water—decreases their ventilation age (*56,57*). In other models, the initial nutrient content of

mode water decreases, leading to a reduction in tropical productivity and, thus, in oxygen demand in the thermocline (*55*). In some longer integrations, deep-ocean overturning ultimately strengthens, raising the oxygen content of the deep waters available to be upwelled into the ODZs (*58*). Given the Plio-Pleistocene stability of the EEP nutrient tongue on >100-kyr timescales, the Pliocene weakening of the ODZ did not appear to derive from reduced nutrient supply to equatorial upwelling system; by elimination, deeper ocean change is implicated (*23,49*). Thus, if the Pliocene is a predictor for ODZ change under global warming, it would argue for an eventual change in interior ocean circulation as one of the salient mechanisms. However, this would only become relevant to future global warming on the multidecadal time scale of mode water ventilation or longer; on decadal timescales or shorter, ODZ changes would be dominated by productivity-driven changes in oxygen demand in the thermocline (*71*). Moreover, the Pliocene results do not rule out more rapid mechanisms of ODZ contraction in response to greater warming, for example, as may have contributed to the ODZ contraction during the Paleocene-Eocene Thermal Maximum (*51*).

References and Notes

1. F. P. Chavez, P. G. Strutton, G. E. Friederich, R. A. Feely, G. C. Feldman, D. G. Foley, M. J. McPhaden, Biological and Chemical Response of the Equatorial Pacific Ocean to the 1997-98 El Niño. *Science* **286**, 2126-2131, doi:10.1126/science.286.5447.2126 (1999).
2. K. E. Trenberth, G. W. Branstator, D. Karoly, A. Kumar, N. C. Lau, C. Ropelewski, Progress during TOGA in understanding and modeling global teleconnections associated with tropical sea surface temperatures. *Journal of Geophysical Research: Oceans* **103**, 14291-14324 (1998).
3. A. Bertrand, et al., *El Niño Southern Oscillation (ENSO) effects on fisheries and aquaculture*. FAO Fisheries and Aquaculture Technical Paper No. 660, Rome, FAO, doi: 10.4060/ca8348en (2020).
4. W. Cai, et al., Changing El Niño-Southern Oscillation in a warming climate. *Nat. Rev. Earth Environ.* **2**, 628-644, doi:10.1038/s43017-021-00199-z (2021).
5. K. D. Burke, J. W. Williams, M. A. Chandler, A. M. Haywood, D. J. Lunt, B. L. Otto-Bliesner, B. L., Pliocene and Eocene provide best analogs for near-future climates. *Proc. Natl. Acad. Sci. U.S.A.* **115**, 13288-13293, doi:10.1073/pnas.180960115 (2018).
6. J. E. Tierney, et al., Past climates inform our future. *Science* **370**, eaay3701, doi:10.1126/science.aay3701 (2020).
7. K. T. Lawrence, Z. Liu, T. D. Herbert, T. D., Evolution of the Eastern Tropical Pacific Through Plio-Pleistocene Glaciation. *Science* **312**, 79-83, doi:10.1126/science.1120395 (2006).
8. P. S. Dekens, A. C. Ravelo, M. D. McCarthy, Warm upwelling regions in the Pliocene warm period. *Paleoceanography* **22**, PA3211, doi:10.1029/2006PA001394 (2007).

9. M. W. Wara, A. C. Ravelo, M. L. Delaney, Permanent El Niño-like conditions during the Pliocene warm period. *Science* **309**, 758-761, doi:10.1126/science.1112596 (2005).

10. Y. Zhang, M. Pagani, Z. Liu, A 12-Million-Year Temperature History of the Tropical Pacific Ocean. *Science* **344**, 84-87, doi:10.1126/science.1246172 (2014).

11. A. C. Ravelo, K. T. Lawrence, A. Fedorov, H. L. Ford, Comment on "A 12-Million-Year Temperature History of the Tropical Pacific Ocean". *Science* **346**, 1467, doi:10.1126/science.1257618 (2014).

12. J. E. Tierney, A. M. Haywood, R. Feng, T. Bhattacharya, B. L. Otto-Bliesner, Pliocene warmth consistent with greenhouse gas forcing. *Geophysical Research Letters*, **46**(15), 9136-9144 (2019).

13. A. V. Fedorov, N. J. Burls, K. T. Lawrence, L. C. Peterson, Tightly linked zonal and meridional sea surface temperature gradients over the past five million years. *Nature Geoscience* **8**, 975-980 (2015).

14. X. Liu, M. Huber, G. L. Foster, A. Dessler, Y. Zhang, Persistent high latitude amplification of the Pacific Ocean over the past 10 million years. *Nat. Commun.* **13**, 7310, doi:10.1038/s41467-022-35011-z (2022).

15. S. M. White, A. C. Ravelo, The benthic B/Ca record at Site 806: new constraints on the temperature of the West Pacific Warm Pool and the "El Padre" state in the Pliocene. *Paleoceanography and Paleoclimatology* **35**(10), e2019PA003812 (2020).

16. J. Bjerknes, Atmospheric teleconnections from the equatorial Pacific. *Monthly Weather Review* **97**(3), 163-172 (1969).

17. S.-P. Xie, S. G. Philander, A coupled ocean-atmosphere model of relevance to the ITCZ in the eastern Pacific. *Tellus A* **46**(4), 340-350 (1994).

18. A. V. Fedorov, P. S. Dekens, M. McCarthy, A. C. Ravelo, P. B. DeMenocal, M. Barreiro, R. C. Pacanowski, S. G. Philander, The Pliocene paradox (mechanisms for a permanent El Niño). *Science* **312**, 1485-1489 (2006).

19. H. L. Ford, A. C. Ravelo, S. Hovan. A deep Eastern Equatorial Pacific thermocline during the early Pliocene warm period. *Earth and Planetary Science Letters* **355**, 152-161 (2012).

20. H. L. Ford, A. C. Ravelo, P. S. Dekens, J. P. LaRiviere, M. Wara, The evolution of the equatorial thermocline and the early Pliocene El Padre mean state. *Geophysical Research Letters* **42**(12), 4878-4887 (2015).

21. Z. Ma, A. C. Ravelo, Z. Liu, L. Zhou, A. Paytan, Export production fluctuations in the eastern equatorial Pacific during the Pliocene-Pleistocene: Reconstruction using barite accumulation rates. *Paleoceanography* **30**, doi:10.1002/2015PA002860 (2015).

22. K. M. Kimble, T. D. Herbert, C. A. Jones, Pliocene weakening of gradients in temperature but not in productivity in the eastern equatorial Pacific. *Paleoceanography and Paleoclimatology* **39**(3), e2023PA004711 (2024).

23. M. G. Shankle, et al., Pliocene decoupling of equatorial Pacific temperature and pH gradients. *Nature* **598**, 457-461, doi:10.1038/s41586-021-03884-7 (2021).

24. Y. G. Zhang, M. Pagani, J. Henderiks, H. Ren, A long history of equatorial deep-water upwelling in the Pacific Ocean. *Earth and Planetary Science Letters* **467**, 1-9 (2017).

25. M. A. Altabet, R. Francois, Sedimentary nitrogen isotopic ratio as a recorder for surface ocean nitrate utilization. *Global Biogeochemical Cycles* **8**, 103-116 (1994).

26. H. Ren, D. M. Sigman, R. C. Thunell, M. G. Prokopenko, Nitrogen isotopic composition of planktonic foraminifera from the modern ocean and recent sediments. *Limnology and Oceanography* **57**(4), 1011-1024 (2012).

27. R. Schiebel, et al., Advances in planktonic foraminifer research: New perspectives for paleoceanography. *Revue de Micropaléontologie* **61** (3-4), 113-138 (2018).

28. R. S. Robinson, et al., A review of nitrogen isotopic alteration in marine sediments. *Paleoceanography* **27**, PA4203, doi:10.1029/2012PA002321 (2012).

29. S. M. Smart, et al., Ground-truthing the planktic foraminifer-bound nitrogen isotope paleo-proxy in the Sargasso Sea. *Geochimica et Cosmochimica Acta* **235**, 463-482 (2018).

30. S. M. Smart, et al., The nitrogen isotopic composition of tissue and shell-bound organic matter of planktic foraminifera in Southern Ocean surface waters. *Geochemistry, Geophysics, Geosystems* **21**(2), e2019GC008440 (2020).

31. P. A. Rafter, C. D. Charles, Pleistocene equatorial Pacific dynamics inferred from the zonal asymmetry in sedimentary nitrogen isotopes. *Paleoceanography* **27**, PA3102, doi: 10.1029/2012PA002367 (2012).

32. P. A. Rafter, D. M. Sigman, C. D. Charles, J. Kaiser, G. H. Haug, Subsurface tropical Pacific nitrogen isotopic composition of nitrate: Biogeochemical signals and their transport. *Global Biogeochemical Cycles* **26**, GB1003, doi:10.1029/2010GB003979 (2012).

33. P. A. Rafter, D. M. Sigman, Spatial distribution and temporal variation of nitrate nitrogen and oxygen isotopes in the upper equatorial Pacific Ocean. *Limnology and Oceanography* **61**, 14–31, doi:10.1002/lno.10152 (2016).

34. C. Wilson, V. J. Coles, Global climatological relationships between satellite biological and physical observations and upper ocean properties. *Journal of Geophysical Research: Oceans* **110**, doi.org/10.1029/2004JC002724 (2005).

35. S. Steph, R. Tiedemann, J. Groeneveld, A. Sturm, D. Nürnberg, Pliocene changes in tropical east Pacific upper ocean stratification: response to tropical gateways?, *in* Tiedemann, R., Mix, A.C., Richter, C., and Ruddiman, W.F. (Eds.), Proc. ODP, Sci. Results 202: College Station, TX (Ocean Drilling Program), 1–51, doi:10.2973/odp.proc.sr.202.211.2006 (2006).

36. S. Steph, et al., Early Pliocene increase in thermohaline overturning: A precondition for the development of the modern equatorial Pacific cold tongue. *Paleoceanography and Paleoclimatology* **25**, https://doi.org/10.1029/2008PA001645 (2010).

37. X. T. Wang, et al., Oceanic nutrient rise and the late Miocene inception of Pacific oxygen-deficient zones. *Proc. Natl. Acad. Sci. U.S.A.* **119**, e2204986119 (2022).

38. J. Marshall, F. Schott, Open-ocean convection: Observations, theory, and models. *Reviews of Geophysics* **37**, 1-64 (1999).

39. J. He, A. Mahadevan, How the source depth of coastal upwelling relates to stratification and wind. *Journal of Geophysical Research: Oceans* **126**, e2021JC017621 (2021).

40. F. Fripiat, et al., The impact of incomplete nutrient consumption in the Southern Ocean on global mean ocean nitrate $\delta^{15}N$. *Global Biogeochemical Cycles* **37**, e2022GB007442 (2023).

41. D. Karl, et al., Dinitrogen fixation in the world's oceans. *Biogeochemistry* **57**, 47-98, doi:10.1023/A:1015798105851 (2002).

42. J. D. Cline, I. R. Kaplan, Isotopic fractionation of dissolved nitrate during denitrification in the eastern tropical North Pacific Ocean. *Mar. Chem.* **3**, 271-299 (1975).

43. J. A. Brandes, A. H. Devol, A global marine-fixed nitrogen isotopic budget: Implications for Holocene nitrogen cycling. *Global Biogeochemical Cycles* **16**, doi:10.1029/2001GB001856 (2002).

44. C. Deutsch, D. M. Sigman, R. C. Thunell, A. N. Meckler, G. H. Haug, Isotopic constraints on glacial/interglacial changes in the oceanic nitrogen budget. *Global Biogeochem. Cycles* **18**, GB4012, doi:10.1029/2003GB002189 (2004).

45. A. Auderset, et al., Enhanced ocean oxygenation during Cenozoic warm periods. *Nature* **609**, 77-82, doi:10.1038/s41586-022-05017-0 (2022).

46. A. Auderset, et al., Sea level modulation of Atlantic nitrogen fixation over glacial cycles. *Paleoceanography and Paleoclimatology* **39**, e2024PA004878 (2024).

47. M. Straub, et al., Changes in North Atlantic nitrogen fixation controlled by ocean circulation. *Nature* **501**, 200-203, doi:10.1038/nature12397.

48. Z. Liu, Z., M. A. Altabet, T. D. Herbert,. Plio-Pleistocene denitrification in the eastern tropical North Pacific: Intensification at 2.1 Ma. *Geochem. Geophys. Geosyst.* **9**, Q11006, doi:10.1029/2008GC002044 (2008).

49. R. S. Robinson, J. Etourneau, P. M. Martinez, R. Schneider, Expansion of pelagic denitrification during early Pleistocene cooling. *Earth Planet. Sci. Lett.* **389**, 52-61, doi:10.1016/j.epsl.2013.12.022 (2014).

50. A. V. Hess, et al., A well-oxygenated eastern tropical Pacific during the warm Miocene. *Nature* **619**, 521-525 (2023).

51. S. Moretti, et al., Oxygen rise in the tropical upper ocean during the Paleocene-Eocene Thermal Maximum. *Science* **383**, 727-731, doi:10.1126/science.adh4893 (2024).

52. T. J. Algeo, P. A. Meyers, R. S. Robinson, H. Rowe, G. Q. Jiang, Icehouse-greenhouse variations in marine denitrification. *Biogeosciences* **11**, 1273-1295, doi:10.5194/bg-11-1273-2014 (2014).

53. C. V. Davis, E. C. Sibert, P. H. Jacobs, N. Burls, P. M. Hull, Intermediate water circulation drives distribution of Pliocene Oxygen Minimum Zones. *Nat. Commun.* **14**, 40, doi:10.1038/s41467-022-35083-x (2023).

54. Y. Takano, T. Ito, C. Deutsch, Projected centennial oxygen trends and their attribution to distinct climate forcings. *Global Biogeochemical Cycles* **32**, 1329-1349 (2018).

55. W. Fu, F. Primeau, J. Keith Moore, K. Lindsay, J. T., Randerson, Reversal of increasing tropical ocean hypoxia trends with sustained climate warming. *Global Biogeochemical Cycles* **32**, 551-564 (2018).

56. J. J. M. Busecke, L. Resplandy, S. J. Ditkovsky, J. G. John, Diverging fates of the Pacific Ocean oxygen minimum zone and its core in a warming world. *AGU Advances* **3**, e2021AV000470 (2022).

57. A. Gnanadesikan, J. L. Russell, F. Zeng, How does ocean ventilation change under global warming? *Ocean Sci.* **3**, 43-53, doi:10.5194/os-3-43-2007 (2007).

58. A. Yamamoto, et al., Global deep ocean oxygenation by enhanced ventilation in the Southern Ocean under long-term global warming. *Global Biogeochemical Cycles* **29**(10), 1801-1815 (2015).

59. J. K. Moore, et al., Sustained climate warming drives declining marine biological productivity. *Science* **359**(6380), 1139-1143 (2018).

60. C. Deutsch, et al., Centennial changes in North Pacific anoxia linked to tropical trade winds. *Science* **345**, 665-668, doi:10.1126/science.1252332 (2014).

61. A. S. Studer, et al., Ice Age-Holocene Similarity of Foraminifera-Bound Nitrogen Isotope Ratios in the Eastern Equatorial Pacific. *Paleoceanography and Paleoclimatology* **36**(5), e2020PA004063 (2021).

62. F. Boscolo-Galazzo, et al., Temperature controls carbon cycling and biological evolution in the ocean twilight zone. *Science* **371**, 1148-1152, doi:10.1126/science.abb6643 (2021).

63. H. L. Ford, N. J. Burls, P. Jacobs, A. Jahn, R. P. Caballero-Gill, D. A. Hodell, A. V. Fedorov, Sustained mid-Pliocene warmth led to deep water formation in the North Pacific. *Nat. Geosci.* **15**, 658-663 (2022).

64. J. B. Novak, R. P. Caballero-Gill, R. M. Rose, T. D. Herbert, H. J. Dowsett, Isotopic evidence against North Pacific Deep Water formation during late Pliocene warmth. *Nat. Geosci.* **17**, 795-802 (2024).

65. Z. Zhang, K. Nisancioglu, U. Ninnemann, Increased ventilation of Antarctic deep water during the warm mid-Pliocene. *Nat. Commun*. **4**, 1499, doi:10.1038/ncomms2521 (2013).

66. L. Bopp, et al., Multiple stressors of ocean ecosystems in the 21st century: Projections with CMIP5 models. *Biogeosciences* **10**, 6225-6245 (2013).

67. J. T. Abell, G. Winckler, R. F. Anderson, T. D. Herbert, Poleward and weakened westerlies during Pliocene warmth. *Nature* **589**, 70-75 (2021).

68. D. M. Sigman, S. L. Jaccard, G. H. Haug, Polar ocean stratification in a cold climate. *Nature* **428**, 59-63 (2004).

69. A. M. de Boer, D. M. Sigman, J. R. Toggweiler, J. L. Russell, Effect of global ocean temperature change on deep ocean ventilation. *Paleoceanography and Paleoclimatology* **22**, PA2210, doi:10.1029/2005PA001242 (2007).

70. W. P. Chaisson, A. C. Ravelo, Pliocene development of the east-west hydrogrpahic gradient in the equatorial Pacific. *Paleoceanography and Paleoclimatology* **15**, 497-505 (2000).

71. N. N. Duprey, et al., Decadal oscillations in the ocean's largest oxygen-deficient zone. *Science* **386**, 1019-1024 (2024).

72. H. E. Garcia, et al., *World Ocean Atlas 2018, Volume 4: Dissolved inorganic nutrients (phosphate, nitrate and nitrate+nitrite, silicate)*. NOAA Atlais NESDIS 84, 35 pp., https://www.nodc.noaa.gov (2018).

73. R. A. Locarini, et al., *World Ocean Atlas 2018, Volume 1: Temperature*. NOAA Atlas NESDIS 81, 52 pp., https://www.nodc.noaa.gov (2018).

74. K. Wyrtki, An estimate of equatorial upwelling in the Pacific. *Journal of Physical Oceanography* **11**, 1205-1214 (1981).

75. European Union-Copernicus Marine Service, *Global Ocean Monthly Mean Sea Surface Wind and Stress from Scatterometer and Model* [Dataset]. Mercator Ocean International. https://doi.org/10.48670/MOI-00181 (2020).

76. K. B. Karnauskas, J. Jakoboski, T. M. S. Johnston, W. B. Owens, D. L. Rudnick, R. E. Todd, The Pacific Equatorial Undercurrent in Three Generations of Global Climate Models and Glider Observations. *J. Geophys. Res.–Oceans*, **125**(11), e2020JC016609, doi: 10.1029/2020JC016609 (2020).

77. A. C. Mix, et al., Benthic foraminifer stable isotope record from Site 849 (0-5-Ma): local and global climate changes. In *Proceedings of the Ocean Drilling Program: Scientific Results* (ed. Pisias, N. G. et al.) vol. 138, 371-412 (1995).

78. L. E. Lisiecki, M. E. Raymo, A Pliocene-Pleistocene stack of 57 globally distributed benthic $d^{18}O$ records. *Paleoceanography* **20**, PA1003 (2005).

79. W. H. Berger, T. Bickert, H. Schmidt, G. Wefer, M. Yasuda, Quaternary oxygen isotope record of pelagic foraminifers: Site 806, Ontong Java Plateau. In *Proceedings ODP: Scientific Results* (ed. Berger, W. H., et al.) vol. 130, 381-395 (1993).

80. E. Jansen, L. A. Mayer, J. Backman, R. M. Leckie, T. Takayama, Evolution of Pliocene climate cyclicity at Hole 806B (5-2 Ma); oxygen isotope record. In *Proceedings ODP: Scientific Results* (ed. Berger, W. H., et al.) vol. 130, 349-362 (1993).

81. D. M. Sigman, et al., A bacterial method for the nitrogen isotopic analysis of nitrate in seawater and freshwater. *Anal. Chem.* **73**, 4145-4153 (2001).

82. A. N. Knapp, D. M. Sigman, F. Lipschultz, N isotopic composition of dissolved organic nitrogen and nitrate at the Bermuda Atlantic Time-series study site. *Global Biogeochemical Cycles* **19**, doi:10.1029/2004GB002320 (2005).

83. H. Ren, et al., Foraminiferal isotope evidence of reduced nitrogen fixation in the ice age Atlantic Ocean. *Science* **323**, 244-248, doi:10.1126/science.1165787 (2009).

84. M. A. Weigand, J. Foriel, B. Barnett, S. Oleynik, D. M. Sigman, Updates to instrumentation and protocols for isotopic analysis of nitrate by the denitrifier method. *Rapid Commun. Mass Spectrom.* **30**, 1365-1383 (2016).

85. J. R. Farmer, A. Martínez-García, L. T. Sentman, R. Schiebel, A. Arns, M. Yehudai, R. Tiedemann, D. M. Sigman, G. H. Haug, Early Pliocene shoaling of the Central American Seaway reconstructed from foraminifera-bound nitrogen and oxygen isotopes. *Paleoceanography and Paleoclimatology* **40**, e2024PA005043 (2025).

86. C. Yoshikawa, T. Nakatsuka, H. Kawahata, Transition of low-salinity water in the Western Pacific Warm Pool recorded in the nitrogen isotopic ratios of settling particles. *Geophysical Research Letters* **32**(14), doi:10.1029/2005GL023103 (2005).

87. P. A. Rafter, D. M. Sigman, K. R. M. Mackey, Recycled iron fuels new production in the eastern equatorial Pacific Ocean. *Nat. Commun.* **8**, 1100, doi:10.1038/s41467-017-01219-7 (2017).

88. J. R. Farmer, et al., Assessment of C, N, and Si isotopes as tracers of past ocean nutrient and carbon cycling. *Global Biogeochemical Cycles* **35**, e2020GB006775 (2021).

89. A. Mariotti, et al., Experimental determination of nitrogen kinetic isotope fractionation—some principles—illustration for the denitrification and nitrification processes. *Plant and Soil* **62**, 413–430 (1981).

90. I. Hansson, A new set of acidity constants for carbonic acid and boric acid in sea water. *Deep Sea Research and Oceanographic Abstracts* **20**, 461-478 (1973).

91. C. Mehrbach, C. H. Culberson, J. E. Hawley, R. M. Pytkowicz, Measurement of the apparent dissociation constants of carbonic acid in seawater at atmospheric pressure, *Limnol. Oceanogr.* **18**, 897–907 (1973).

92. F. J. Millero, The thermodynamics of the carbonate system in seawater. *Geochimica et Cosmochimica Acta* **43**, 1651-1661 (1979).

93. A. G. Dickson, F. J. Millero, A comparison of the equilibrium constants for the dissociation of carbonic acid in seawater media, *Deep-Sea Res.* **34**, 1733–1743 (1987).

94. T. J. Lueker, A. G. Dickson, C. D. Keeling, Ocean pCO_2 calculated from dissolved inorganic carbon, alkalinity, and equations for K_1 and K_2: validation based on laboratory measurements of CO_2 in gas and seawater at equilibrium. *Mar. Chem.* **70**, 105–119 (2000).

95. R. E. Zeebe, D. Wolf-Gladrow, *CO_2 in seawater: equilibrium, kinetics, isotopes*, Elsevier Science, Amsterdam (2001).

96. E. R. Lewis, D. W. R. Wallace, Program developed for CO_2 system calculations (CO2SYS). ORNL/CDIAC-105, Carbon Dioxide Information Analysis Center, Oak Ridge National Laboratory, U.S. Department of Energy, Oak Ridge, Tennessee (1998).

97. B. R. Carter, et al., Pacific anthropogenic carbon between 1991 and 2017. *Global Biogeochemical Cycles* **33**, 597–617, https://doi.org/10.1029/2018GB006154 (2019).

98. R. P. Caballero-Gill, T. D. Herbert, H. J. Dowsett, 100-kyr paced climate change in the Pliocene warm period, Southwest Pacific. *Paleoceanography and Paleoclimatology* **34**(4), 524-545 (2019).

99. R. Schlitzer, Ocean Data View (2025); https://odv.awi.de

100. P.A. Rafter, D.M. Sigman, J.R. Farmer, NOAA/WDS Paleoclimatology – Equatorial Pacific foram-bound N isotopes from the Pliocene to the Pleistocene. *National Centers for Environmental Information* (2021), doi:10.25921/4kp0-q894.

Acknowledgments: P.A.R. is grateful for early, consistent, and persistent support from L. Aluwihare and C. Charles. Critical analytical support was provided by X. Xu, D. Zhang, J. Southon, S. Oleynik, and many UC Irvine undergraduate student researchers. The authors are also thankful for comments from three anonymous reviewers. **Funding:** National Science Foundation grant OCE-1635610 (PAR), OCE-2303549 (JRF), and OCE-2303548 (DMS); the Tuttle Fund of the Department of Geosciences, Princeton University (D.M.S.); and the Max Planck Society (G.H.H., A.M.-G.). **Author contributions:** Conceptualization: PAR, JRF, AMG, DMS; Methodology: PAR, JRF, AMG, DMS, HR, SB; Investigation: PAR, JRF, DMS, ACR, KK; Visualization: PAR, JRF; Funding acquisition: PAR, DMS, GHH, ACR; Project administration: PAR, JRF, DMS; Supervision: PAR, JRF, DMS; Writing – original draft: PAR, JRF, DMS; Writing – review & editing: PAR, JRF, AMG, ACR, KK, AA, FB, DMS, HR, SB, GHH**. Competing interests:** Authors declare that they have no competing interests. **Data and materials availability:** All data are available in the main text or the supplementary materials or at the National Centers for Environmental Information (*100*)

Supplementary Materials

Materials and methods

Figs. S1 to S6

Table S1

Data S1-S5

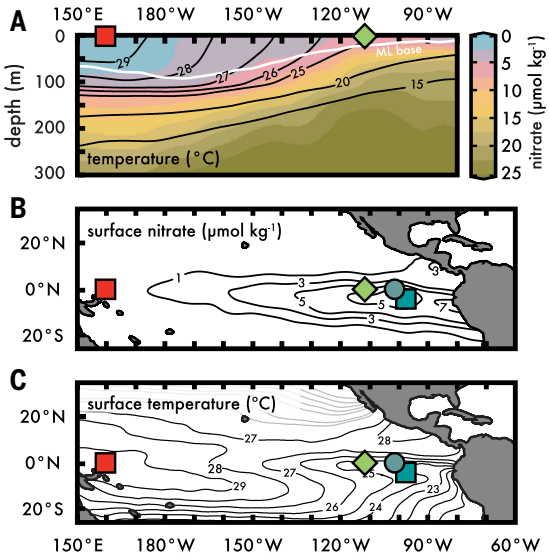

Fig. 1. Upwelling brings cool, nutrient-rich water to the eastern Equatorial Pacific surface. (**A**) The strong coupling between equatorial Pacific temperature (contoured) and nitrate concentration (colors) within the upper water column. The white line is an estimate of the annual surface ML base depth, here equal to a 0.75°C difference from the local SST. (**B** and **C**) Surface annual average (B) nitrate concentrations (*73*) and (C) temperature (*72*) show the extent of cool, nitrate-rich surface ocean waters upwelled in the eastern Equatorial Pacific. Symbols in (A) to (C) show ODP Sites 806 (red square), 849 (green diamond), 847 (blue circle, 0.2°S, 95.3°W;

3334 m depth), and 846 (blue square, 3.1˚S, 90.8˚W, 3296 m depth). DSDP Site 516 (30.3˚S, 35.3˚W, 1313 m depth) is not shown. Figure prepared using Ocean Data View (*99*).

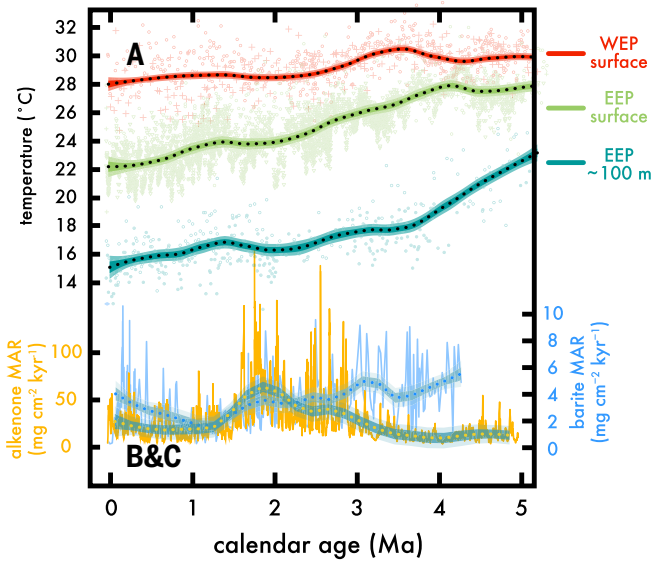

Fig. 2. SST across the tropical Pacific and shallow subsurface temperature and productivity in the EEP since the warm Pliocene. (**A**) Published SST estimates for the WEP (top) and EEP (middle) using *T. sacculifer* Mg/Ca [circles (*9*)], TEX_{86} [pluses (*10,14*)], and alkenones [triangles (*7,8*)]. EEP shallow subsurface (~ 100 m) temperature is the bottom line in (A) and uses *G. tumida* Mg/Ca (*19,20*). (**B** and **C**) EEP productivity from mass accumulation rates (MAR) of (B) alkenone abundance [yellow, left axis (*7*)] and (C) barite [cyan, right axis (*21*)]. Dotted lines show LOESS-averaged temperature and productivity reconstructions for all data with shaded regions indicating ±1 and ±2 SE (Materials and methods).

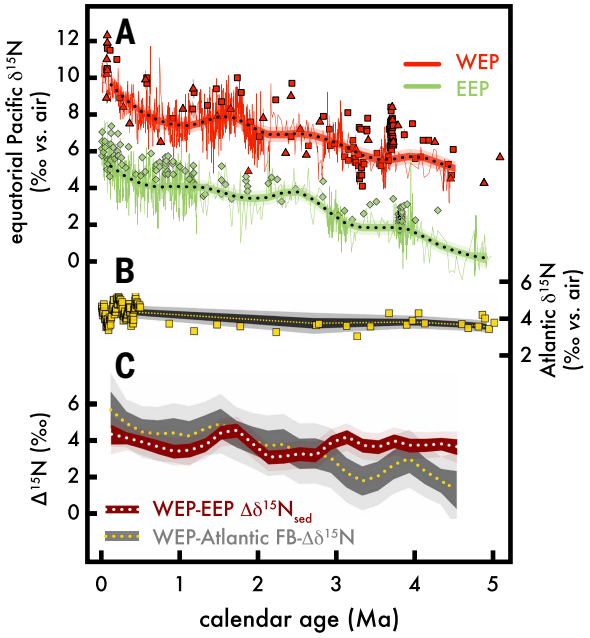

Fig. 3. Nitrogen isotopes across the tropical Pacific since the warm Pliocene, east-west differences, and comparison with the South Atlantic. (**A**) Bulk sediment $\delta^{15}N$ (red line), FB-$\delta^{15}N$ in *T. sacculifer* (squares), and FB-$\delta^{15}N$ in *Globigerinoides ruber* (triangles) are from ODP site 806; bulk sediment $\delta^{15}N$ (green line) and FB-$\delta^{15}N$ in *G. menardii* or *G. tumida* (diamonds) are from ODP site 849. EEP FB-$\delta^{15}N$ values are lowered by 0.88 per mil to correct for a known species-specific offset (Materials and methods). (**B**) FB-$\delta^{15}N$ in *T.sacculifer* from South Atlantic DSDP site 516 [yellow; (*45,46*)]. LOESS trends ±1 SE are shown as dots and colored envelopes for bulk sediment $\delta^{15}N$ in (A) and FB-$\delta^{15}N$ in (B). (See fig. S2 for alternate LOESS trends and $\Delta\delta^{15}N$ values.) (**C**) $\delta^{15}N$ differences (as $\Delta\delta^{15}N$) between WEP $\delta^{15}N_{sed}$ and EEP $\delta^{15}N_{sed}$ (red) and between WEP FB-$\delta^{15}N$ and South Atlantic FB-$\delta^{15}N$ (gray). LOESS trends are shown as dots with the ±1 and ±2 SE shown as colored envelopes for bulk sediment $\delta^{15}N$ in (A), FB-$\delta^{15}N$ in (B) and $\Delta\delta^{15}N$ in (C). (See fig. S2 for alternate LOESS trends and $\Delta\delta^{15}N$ calculations.)

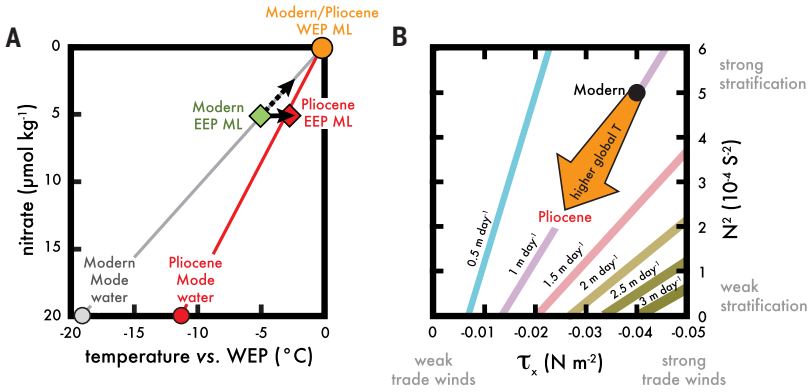

Fig. 4. Role of subsurface warming in explaining Pliocene EEP nutrient conditions and temperature. (**A**) Simplification of the EEP as the product of two-component mixing between tropical Pacific surface waters (top, based on the WEP surface) and subsurface mode waters (bottom) yields distinct nitrate versus temperature relationships for modern (gray, left) and Pliocene conditions (red, right) (Materials and methods and fig. S6). Black arrows demonstrate two potential ways to change the temperature and nitrate properties of the modern EEP ML (green diamond). The dashed arrow illustrates that, given the modern endmembers, reducing the proportion of newly supplied thermocline water to the EEP ML (e.g., slowing the upwelling rate and/or deepening the ML) would also lower the ML nitrate concentration, counter to the N-isotope data. By contrast, with a higher temperature and a conserved nitrate concentration for Pliocene mode waters (see main text), warming of the EEP ML is achieved without decreasing its nitrate concentration (horizontal black arrow and red diamond), in agreement with the stable zonal $\delta^{15}N$ gradient (Fig. 3). Although a two-component mixing model is clearly a vast oversimplification of the tropical Pacific system, relevant missing processes appear unlikely to nullify its implications (Materials and methods). (B) Ekman upwelling vertical velocity (contours) as a function of zonal wind stress (τ_x) and buoyancy frequency squared (N^2), an indicator of stratification, calculated with a box model of the equatorial Pacific (*74*). Vertical velocity is calculated as Ekman pumping velocity damped by stratification (Materials and methods). The point labeled "Modern" indicates τ_x averaged ±2° latitude across the equator in the WEP (160°E to 160°W) (*76*) and N^2 averaged ±2° latitude across the equator in the EEP (93°W) (*75*). The orange arrow indicates that the combination of weaker trade winds (lower absolute τ_x) and reduced upper-ocean stratification (lower N^2) could have maintained upwelling velocity in the EEP during the warm Pliocene.